Hindawi
Advances in Materials Science and Engineering
Volume 2018, Article ID 7679131, 9 pages
https://doi.org/10.1155/2018/7679131

Research Article

Water Absorption Properties of Cement Pastes: Experimental and Modelling Inspections

Ludovica Casnedi, Ombretta Cocco, Paola Meloni, and Giorgio Pia

Dipartimento di Ingegneria Meccanica, Chimica e dei Materiali, Università degli Studi di Cagliari, Piazza d'Armi, 09123 Cagliari, Italy

Correspondence should be addressed to Giorgio Pia; giorgio.pia@dimcm.unica.it

Received 15 September 2017; Revised 15 November 2017; Accepted 4 December 2017; Published 13 February 2018

Academic Editor: Renal Backov

An intermingled fractal units' model is shown in order to simulate pore microstructures as pore fraction and pore size distribution. This model is aimed at predicting capillary water absorption coefficient and sorptivity values in cement pastes. The results obtained are in good agreement with the experimental ones. For validating this model, a comparison with other procedures has been shown. It is possible to establish that the newly proposed method matches better with the experimental results. That is probably due to the fact that pore size distribution has been considered as a whole. Moreover, even though the proposed model is based on fractal base units, it is able to simulate and predict different properties as well as nonfractal porous microstructure.

1. Introduction

Porous building materials may suffer from weathering process caused by physical, chemical, and biological factors [1, 2]. The influence of these deterioration processes depends on the *topoclimatic* environmental conditions, the material type, its preservation state, and location on the building [3, 4].

The circulation of water within microstructures of porous materials causes them to deteriorate considerably more rapidly, consequently compromising their behaviour [5–7]. Their thermal (insulation) performance, mechanical properties, and degradation kinetics are therefore proportional to the amount of water that they may contain.

For this reason, the study of the capillary suction properties of construction materials remains a matter much debated [8–13]. Its importance is connected to the analysis of their performance when installed as well as their durability [14–16]. In order to preserve these materials, it is necessary, in particular when it comes to historical building, to apply inspection methods, which not only assess the conservation state of the microstructure of materials but also help in the future evolution of a number of characteristics related to porosity for traditional or advanced engineering applications [17–21].

In this regard, a large number of studies have dealt with these properties using several modelling procedures [9, 12, 22]. Over the last few decades, a new type of geometrical analysis has been developed which utilises figures with fractional dimensions, known as *fractals*. This term is derived from the Latin word *fractus* (broken/fractured). The importance of this approach is due to its usefulness in describing the analysis of complex systems. According to Mandelbrot, there are a large number of fractals in nature and these forms may be used for describing some common aspects such as vegetables' growth, mountains and rivers geomorphology, geometrical organisation of human organs, and in our case, materials' microstructures [23]. A fractal (deterministic fractal) is a geometric figure whose each and every part is similar to the whole and is repeated on different scales (self-similarity and autosimilarity). Many fractals are constructed using the iteration procedure. For example, the well-known Menger sponge is created by splitting each of the edge of the primary solid cube into three equal parts, creating 27 subcubes. Seven of these subcubes will be removed: the subcube in the middle of each face and the subcube in the

centre of the cube. For the later iterations, which can be infinite, the same subdivision and removal process are repeated on the remaining solid subcubes.

In microstructure modelling terms, the development of a fractal, as the Menger sponge, is dimensionally limited to the measurements of the edge of the larger and smaller cubes. While the number of iteration increases, geometrical structure is fine, highly intricate, and detailed at all scales. When it comes to porosity, fractal geometry displays a well-known series of "sponges" that, regardless of being originally very simple, recall the pore size distribution or the morphology of their outlines (e.g., the Menger sponge or its corresponding bidimensional model known as the Sierpinski carpet).

The development into space of the scaling procedures (self-similarity, applied on no less than two/three orders of magnitude) allows the process of the porosimetric data obtained by mercury intrusion porosimetry or gas absorption. These applications can be found in the literature in several different cases and include traditional as well as the study of advanced ceramic materials, namely, sandstones and soils as well as cement materials [24–27].

Quite recently, it has also been possible to connect the fractal geometry to a number of relations enabling the effective and rational (not empirical) evaluation of physical quantities which are technologically relevant [5, 28, 29].

For example, Winslow [30] described the X-ray scattering technique for measuring the dimension of a fractal surface to demonstrate that the surface of hydrated cement paste is fractal in character and has a large fractal dimension. A model to describe nucleation and growth for the hydration of tricalcium silicate has been presented by Livingston [31]. Lange et al. [32] explored several image analysis techniques that provide insight into the nature of pore structure as observed in backscattered electron images of polished sections. Diamond and Bonen [33] have shown that pore systems of concrete may present fractal characteristics. In the study by Arandigoyen and Alvarez [34], the microstructure of blended mortars is studied taking into account porosity and pore size distributions. Surface fractal dimension has been calculated and correlated with the percentage of cement/lime. It has been shown that the system with higher percentage of cement has higher surface fractal dimension values. Comegna et al. [35] used "Tyler and Wheatcraft fractal model" for determining soil-water retention curves. Meanwhile, in Xu and Dong [36], the soil-water characteristics, hydraulic conductivity, and soil-water diffusivity of unsaturated soils are derived and expressed by only two parameters, the fractal dimension and the air-entry value, which can be evaluated from the fractal model for the pore size distribution. In [37], Shi et al. presented a series of fractal models developed to investigate the effect of gas diffusion layer's wettability on liquid water and gas permeation. Zheng and Yu [38] proposed a fractal analytical expression in order to predict gas permeability flow through dual-porosity media. The model predictions are in good agreement with the experimental data. Furthermore, the fractal geometry has been used to correlate mechanical behaviour and thermal conductivity with pore size distribution [29, 39–44].

This paper is set out to highlight that, through appropriate fractal modelling techniques applied to the microstructure derived from experimental tests requiring a fairly small amount of material, such as mercury intrusion techniques, it is possible to predict the water content that such microstructures absorb as a function of the exposed surface and the time of exposition: sorptivity coefficient.

Moreover, fractal model data are compared with other models from [9, 12].

The purpose of this communication, in addition to illustrating how experimental data on capillary suction correspond very closely to those obtained from the intermingled fractal unit (IFU) model, is to put forward the idea of developing a new model which is able to predict the properties which are connected to the microstructure in any porous material [5, 42, 44]. In a former article, it was noted how the IFU and the fractal procedure are able to get some values of thermal conductivity and mechanical properties which are very close to those obtained experimentally [29, 43, 44]. For this reason, this approach could be a very useful tool to design cement pastes and concrete materials with peculiar physical properties.

2. IFU Model and Analytical Expression for Calculating Sorptivity Coefficient

The proposed model is based on the Sierpinski carpets as base units. This fractal figure is obtained by commencing from a square with sides which are divided according to a factor (F) of 3, resulting into a figure consisting of 9 subsquares, from which two are removed. The remaining 7 subsquares (s) are treated in the same manner; that is, their sides are divided by the length scale factor (F) of 3, thus generating a further 9 subsquares, from which 2 are removed (Figure 1(a)) and 7 are involved in the iteration process. This procedure may continue *ad infinitum*, but for experimental cases, the number of iterations (i) depends on the porosimetric range (Figure 1(a)). Fractal dimension of the figure under consideration is calculated as

$$D_f = \frac{\log(s)}{\log(F)}. \tag{1}$$

Different Sierpinski carpets can be obtained by changing the number of the removed squares or the number of iterating and noniterating squares. An example of this configuration is shown in Figure 1(b). It is possible to note that there are 5 iterating squares and 2 *solid forever* squares at second iteration. This configuration is repeated for the following iterations.

The extruded Sierpinski carpet has a pore size distribution in which the hypothetical mercury volume intruded is proportional to pore size. The maximum adsorption corresponds to maximum pore ray. Porous materials can have a more complex pore size distribution in which maximum pores coincide with a generic pore radius or there may be more peaks corresponding to the pore size of the radius range [45]. In both cases, these pore size distributions are not typically fractal.

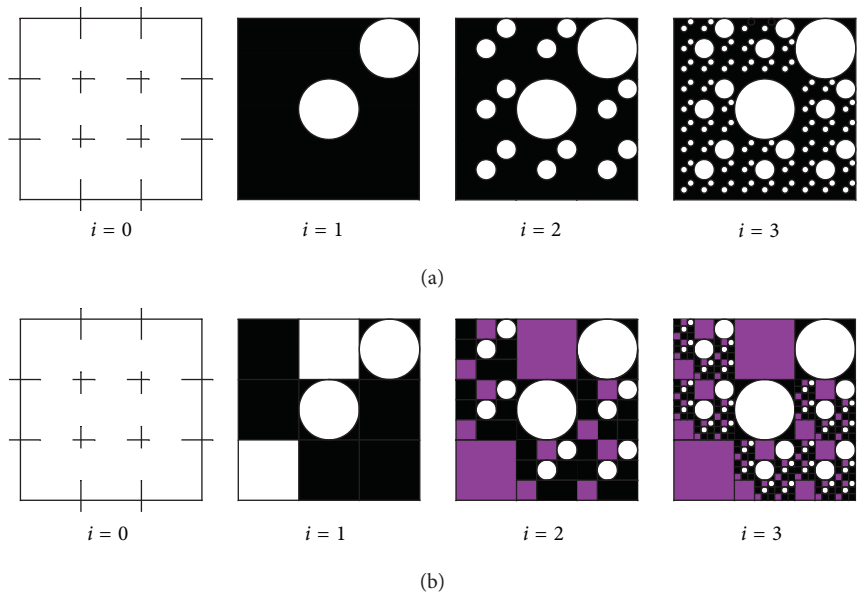

FIGURE 1: Sierpinski carpet construction: (a) geometric construction of the Sierpinski carpet and its iteration process. The fractal dimension D_f is 1.77 and the iterations are 3. (b) Fractal scaling ($i = 0$, 1, 2, and 3) for the Sierpinski carpet with two pores at first iteration. Starting from second iteration, two squares remain *solid forever* and five squares generate new iteration.

It has recently been shown that even real nonfractal structures can be effectively modelled by laying together different fractal units. This modelling procedure, called intermingled fractal unit (IFU) model, is able to reproduce porous microstructure in terms of agreement with experimental porosimetric data: pore volume fraction (ε_{exp}) and pore size distribution [28, 44] (Figure 2).

Considering the value of ε, obtained from the MIP tests, in a simple case in which only two different types of the Sierpinski carpet have been utilised as base units, the number n_B of B base units, for each A base unit, is calculated by the equation

$$n_B = \frac{\left(A_{Ap} - \varepsilon_{\text{exp}} \cdot A_A\right)}{\left(\varepsilon_{\text{exp}} \cdot A_B - A_{Bp}\right)}, \tag{2}$$

where A_A, A_B, A_{Ap}, and A_{Bp} represent the total areas and the total pore areas of units A and B (Figure 2).

The base units have different maximum pore sizes, whereas they could have different numbers of removed squares as well as fractal dimension, iterations, pore volume fraction, etc.

In order to gain control on the pore fraction value, it could be necessary to introduce sufficient parts of IFU-*filled surface*. This part of the model is not involved in any pore generation process and is porosity free. So, whenever useful, it is possible to keep porosity constant by varying the pore size distribution. For the same reason, as shown in Figure 1(b), some squares derived from the Sierpinski carpet cannot be part of the iteration process, thus remaining *solid forever* (no porosity). In order to obtain a tridimensional model, the Sierpinski carpets and filled surface are extruded connecting in series more IFU cross sections. The mercury intrusion porosimetric (MIP) technique, from which, in this work, experimental data are acquired, considers separate and distinct capillaries. For this reason, in the proposed model, no connections in any directions are considered. However, capillary rise is perturbed by pore tortuous paths decreasing fluid rate.

At the same time, the obtained IFU arrangement must be considered from analytical point of view. In this sense, for reproducing porous microstructures, it is sufficient to know the numerical characteristics of the base units and the filled surface. Geometrical representations, as reported in Figure 2, are oversimplified scheme (e.g., n_B is a very large value, i.e., $\approx 10^9$, which results into nonfit for the illustration purpose).

Overall, all these model characteristics make it particularly performing and sensitive with regard to the most different pore size distributions experimentally verifiable.

During the water capillary absorption process, the sorptivity value is represented by the slope of the rectilinear section of the curve between water absorption per unit area versus square root of time. Each class of pores, therefore, absorbs at its own speed as a function of the radius size. In order to calculate the sorptivity so that it can be compared with experimental values, it is necessary to study the flow of fluid which passes through every base units of IFUs.

In a porous model with the characteristics expressed above, the number of pores for a given iteration, i, is given by the following formula:

$$N_{\text{pores}\,(i=n)} = F^{i \cdot D_f}\left(F^{2-D_f} - 1\right). \tag{3}$$

If $i = 2$, $F = 3$, and $D_f = 1.77$, then $N_{\text{pores}\,(i=n)} = 3^{2 \cdot 1.77}\,(3^{2-1.77} - 1) = 14$, as shown in Figure 1(a), indeed the second iteration generates 14 new pores.

The flow of a fluid for an individual capillary with a section calculated as that of the circumference inscribed in

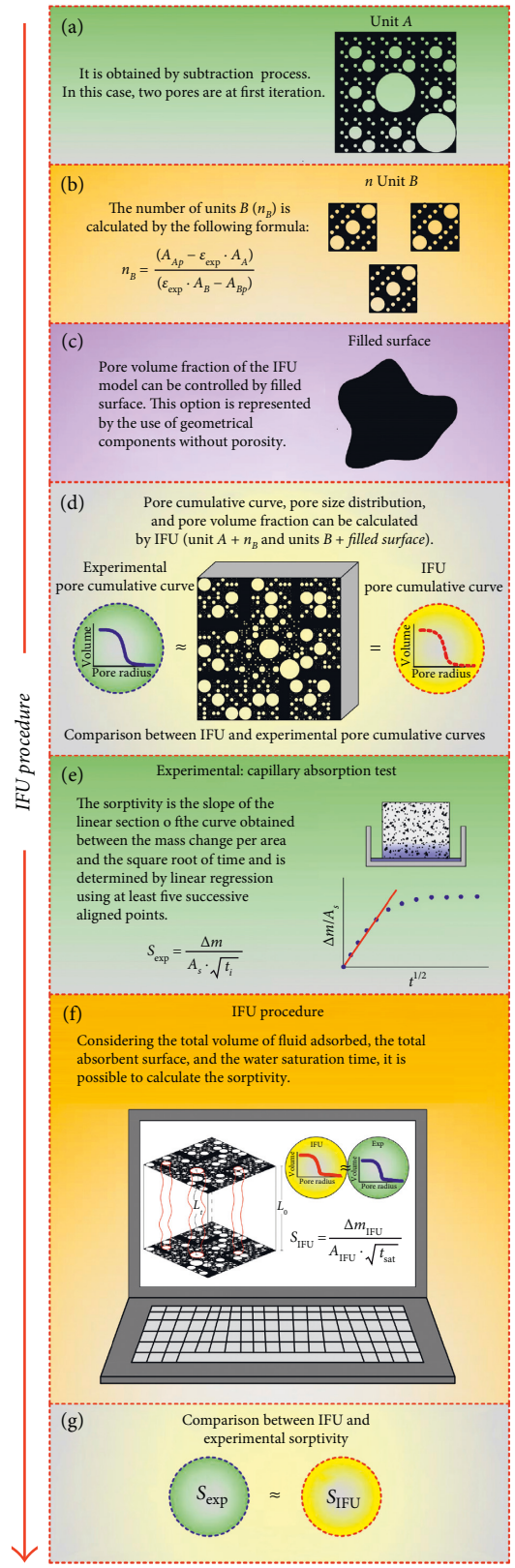

Figure 2: Modelling procedure to calculate the sorptivity value. (a) to (c) IFU construction intermingling different types and numbers of the Sierpinski carpets and solid surface; (d) comparison between experimental and IFU pore cumulative curves; (e) and (f) calculation of sorptivity applying the fractal expression; (g) comparison between experimental and model sorptivity data.

the square subtracted from the given iteration i is given by the Hagen-Poiseuille equation:

$$q(\lambda) = \frac{\pi}{128} \frac{\Delta p}{L_t(\lambda)} \frac{\lambda^4}{\mu}, \tag{4}$$

where Δp is the pressure loss, L_t is the capillary length considering tortuosity, λ is the pore diameter, and μ is the dynamic viscosity.

The tortuous path of pores (L_t) is expressed by

$$L_t(\lambda) = L_0^{D_t} \lambda^{1-D_t}, \tag{5}$$

where L_0 is the length of rectilinear capillary and its value corresponds to the dimension (height) of the sample and D_T is the tortuous fractal dimension:

$$D_T = 1 + \frac{\ln \tau}{\ln(L_0/\lambda)}. \tag{6}$$

τ_{class} is the tortuosity of the specific pore class, calculated as

$$\tau_{class} = 1 + a \ln \frac{1}{\varepsilon_{class}}, \tag{7}$$

where ε_{class} is the pore class volume fraction and a is a constant that depends on pore shape (in this case, its value is 0.63) [46].

Moreover, a generic diameter may be expressed by the following relation:

$$\lambda = \frac{\lambda_{max}}{F^{(i-1)}}. \tag{8}$$

Simple algebra shows that the Hagen-Poiseuille equation can be rewritten as

$$q_{pore}(\lambda) = \frac{\pi}{128} \frac{\Delta p}{L_t} \frac{1}{\mu} \frac{\lambda_{max}^4}{F^{4(i-1)}}. \tag{9}$$

The flow Q_{class} for a generic class of pores is the result of $q_{pore} \cdot N$, thus,

$$Q_{class} = \left(\frac{\pi}{128} \frac{\Delta p}{L_t} \frac{1}{\mu} \frac{(\lambda_{max})^4}{F^{4(i-1)}} \right) \cdot \left(F^{i \cdot D_f} \left(F^{2-D_f} - 1 \right) \right). \tag{10}$$

The average speed of water rising A_p as total porous surface will be given by

$$v = \frac{Q}{A_p}, \tag{11}$$

where Q is the total flow and A_p is the total porous surface.

In this manner, the time that the fluid takes to saturate each single pore could be obtained by the following equation:

$$t_{sat} = L_0 \left\{ \frac{1}{A_p} \left(\frac{\pi}{128} \frac{\Delta p}{L_t(\lambda)} \frac{1}{\mu} \frac{(\lambda_{max})^4}{F^{4(i-1)}} \right) \cdot \left[F^{i \cdot D_f} \left(F^{2-D_f} - 1 \right) \right] \right\}^{-1}. \tag{12}$$

At time $t_{\lambda sat}$ of the most significant class of pores for capillary absorption, it is possible to calculate all the heights

Table 1: IFU input data to models A-1 and A-2. The fractal dimension (D_f), the maximum (R_{max}) and minimum rays (R_{min}), the number of iterations, the number of solid forever squares for each base unit (the Sierpinski carpet), the number of B base units (n_B), the filled surface (FS) used to build the IFU, and comparison between experimental (ε_{exp}) and predicted pore volume fractions (ε_{IFU}).

		A-1	A-2
Unit *A*	D_f	1.89	1.89
	n	1	1
	R_{max} (μm)	1.50	40
	Iteration	1	8
	R_{min} (μm)	0.5	0.06
	Solid forever	0	1
Unit *B*	D_f	1.77	1.77
	n	31	1991
	R_{max} (μm)	0.3	1.48
	Iteration	4	5
	R_{min} (μm)	0.004	0.06
	Solid forever	0	0
	Filled surface (μm^2)	0	$1.36{\cdot}10^4$
	$\varepsilon_{exp}/\varepsilon_{calc}$	0.36/0.36	0.65/0.65

Table 2: IFU input data to models B-1, B-2, and B-3. The fractal dimension (D_f), the maximum (R_{max}) and minimum rays (R_{min}), the number of iterations, the number of solid forever squares for each base unit (the Sierpinski carpet), the number of B base units (n_B), the filled surface (FS) used to build the IFU, and comparison between experimental (ε_{exp}) and predicted pore volume fractions (ε_{IFU}).

		B-1	B-2	B-3
Unit *A*	D_f	1.63	1.89	1.77
	N	1	1	1
	R_{max} (μm)	2.88	7.39	5.87
	Iteration	6	7	6
	R_{min} (μm)	0.004	0.003	0.008
	Solid forever	2	0	4
Unit *B*	D_f	1.63	1.89	1.77
	N	$6.77{\cdot}10^8$	$1.62{\cdot}10^7$	$7.79{\cdot}10^5$
	R_{max} (μm)	0.04	0.03	0.07
	Iteration	2	2	2
	R_{min} (μm)	0.004	0.003	0.008
	Solid forever	4	4	1
	Filled surface (μm^2)	$8.70{\cdot}10^7$	$5.29{\cdot}10^5$	$4.08{\cdot}10^4$
	$\varepsilon_{exp}/\varepsilon_{calc}$	0.11/0.11	0.19/0.19	0.37/0.37

reached by the fluid on the remaining pores of different radii (eventually, for the pores higher than the representative radius, at $t_{\lambda sat}$, they are considered filled of water).

Consequently, the volume of fluid absorbed could be calculated by

$$V_{tot} = \sum_{1}^{n} A_p \cdot h_{class}. \tag{13}$$

Considering the mass of the total volume of absorbed water, $\Delta m_{IFU} = V_{tot} \cdot \rho$, in which ρ is the density of water and the total absorbent surface (A_{IFU}) sorptivity is equal to

Table 3: IFU input data to models C-1, C-2, C-3, and C-4. The fractal dimension (D_f), the maximum (R_{max}) and minimum rays (R_{min}), the number of iterations, the number of solid forever squares for each base unit (the Sierpinski carpet), the number of B base units (n_B), the filled surface (FS) used to build the IFU, and comparison between experimental (ε_{exp}) and predicted pore volume fractions (ε_{IFU}).

		C-1	C-2	C-3	C-4
Unit *A*	D_f	1.89	1.89	1.89	1.89
	N	1	1	1	1
	R_{max} (μm)	54.66	36	45	60.66
	Iteration	10	9	10	10
	R_{min} (μm)	0.003	0.002	0.002	0.002
	Solid forever	0	0	0	1
Unit *B*	D_f	1.63	1.63	1.77	1.77
	N	$1.13{\cdot}10^9$	$4.43{\cdot}10^7$	$41.75{\cdot}10^8$	$1.49{\cdot}10^8$
	R_{max} (μm)	0.008	0.016	0.021	0.028
	Iteration	2	2	3	3
	R_{min} (μm)	0.003	0.002	0.002	0.002
	Solid forever	4	3	3	3
	Filled surface (μm^2)	$4.41{\cdot}10^6$	$5.77{\cdot}10^5$	$3.71{\cdot}10^6$	$1.82{\cdot}10^6$
	$\varepsilon_{exp}/\varepsilon_{calc}$	0.17/0.17	0.23/0.23	0.21/0.21	0.27/0.27

$$S_{IFU} = \frac{\Delta m_{IFU}}{A_{tot} \cdot \sqrt{t_{\lambda sat}}}. \tag{14}$$

In brief, the use of the IFU consists of (Figure 2 shows an outline about IFU sorptivity procedure) (a) cumulative MIP curve data analysis and verification of the fractality of the microstructures [44, 47], (b) model processing (based on the Sierpinski carpets with different geometric size and scaling iterations) in order to reproduce the experimental pore size distribution and the pore volume fraction, (c) applying the fractal expression of capillary adsorption for each unit and considering the various contributions, and (d) comparison between modelling predictions and experimental and/or other model soptivity data [9, 12].

3. Materials

3.1. First Data Set (A). The microstructures analysed are systems with a cementitious CPA CEM I 52.5 (EN 196-1) and argillaceous matrix consisting exclusively of kaolin (with an absolute density, measured using a water pycnometer, of 2.65 g/cm^3) [48, 49]. The wood aggregates (*Picea* wood) have sizes between 3 and 8 mm: A-1 (clay cement matrix) and A-2 (clay cement matrix + 30% wood aggregates). Samples are placed in a storage room for 28 days.

3.2. Second Data Set (B). A commercial Portland cement CEM II 42.5 to make up pastes with water-cement rations (w/c; by weight) of 0.25, 0.34, and 0.43 is used (henceforward referred to as B-1, B-2, and B-3) [50]. The test specimens (25 mm cubes) were aged for 28 days (7 days under water and 21 days in air).

Table 4: IFU input data to models D-1, D-2, D-3, D-4, D-5, and D-6. The fractal dimension (D_f), the maximum (R_{max}) and minimum rays (R_{min}), the number of iterations, the number of solid forever squares for each base unit (the Sierpinski carpet), the number of B base units (n_B), the filled surface (FS) used to build the IFU, and comparison between experimental (ε_{exp}) and predicted pore volume fractions (ε_{IFU}).

		D-1	D-2	D-3	D-4	D-5	D-6
Unit *A*	D_f	1.89	1.89	1.77	1.63	1.77	1.89
	N	1	1	1	1	1	1
	R_{max} (μm)	2.25	7	19	18	34	34
	Iteration	7	8	9	9	9	9
	R_{min} (μm)	0.002	0.002	0.002	0.002	0.002	0.002
	Solid forever	0	5	4	4	6	0
Unit *B*	D_f	1.89	1.89	1.63	1.63	1.46	1.46
	N	$5.05{\cdot}10^4$	$1.38{\cdot}10^5$	$9.78{\cdot}10^5$	$9.32{\cdot}10^5$	$7.39{\cdot}10^5$	$3.19{\cdot}10^5$
	R_{max} (μm)	0.083	0.086	0.078	0.074	0.14	0.14
	Iteration	4	4	4	4	4	4
	R_{min} (μm)	0.002	0.002	0.002	0.002	0.002	0.002
	Solid forever	2	1	2	2	3	3
	Filled surface (μm^2)	$4.10{\cdot}10^8$	$7.89{\cdot}10^8$	$1.26{\cdot}10^5$	$4.13{\cdot}10^4$	$4.67{\cdot}10^4$	0
	$\varepsilon_{exp}/\varepsilon_{calc}$	0.22/0.22	0.29/0.29	0.37/0.37	0.48/0.48	48.7/48.7	0.60/0.60

3.3. Third Data Set (C). Four cement-based mortars, hereafter referred to as C-1, C-2, C-3, and C-4, are considered [51]. All the composites were produced on the basis of the Portland cement CEM I 42.5 R, natural quartz sand with maximum grain size of 2 mm (from Bielinek in Poland), and tap water in different quantities. The weight ratio of sand and binder (cement, silica fume) was s : b = 3.1 : 1.0. Curing was performed for 28 days in air (lab conditions).

3.4. Fourth Data Set (D). Sixty cylindrical specimens of 4 cm (diameter of 3.4 cm) were elaborated blending the lime with the cement in order to obtain six different compositions (% lime: 0, 20, 40, 60, 80, and 100%, resp., called D-1, D-2, D-3, D-4, D-5, and D-6) with 10 specimens of each composition [52]. Different amounts of mixing water were employed in order to obtain a similar consistency in all the pastes. The specimens, arranged in a vertical position, were cured in ambient laboratory conditions (RH $60 \pm 10\%$ and $20 \pm 5^{\circ}$C) for 2 years. Other characteristics are illustrated in the reference.

For all systems, capillary absorption and mercury intrusion porosimetry (MIP) tests to measure sorptivity values and porosity (pore size distribution and pore size range) have been conducted [48–52].

Capillary tests are performed placing regular specimens in a container with a dry bedding layer (minimum thickness of 5 mm). During absorption, water must be added in order to maintain the water-level constant. Samples are weighed at regular interval, which depends on the speed of water absorption. When the weight of the samples remains constant (±1%) for 24 hours, the test is ended.

The water absorbed per unit of exposed surface Q_i (mg/cm^2) at time t_i (s) is estimated by using $Q_i = [(m_i - m_0)/A_s]$, in which m_i (mg) is the mass of the sample at time t_i, m_0 (mg) is the mass of the dry specimen, and A_s (cm^2) is the area of the sample face in contact with the water layer.

The capillary water absorption coefficient (S_{exp}), also called *sorptivity*, is defined as the slope of the linear section of the curve obtained by reporting in a plot the mass variation per area (Q_i) versus the square root of time ($t_i^{1/2}$) and was determined by linear regression using at least 5 successive aligned points.

Mercury intrusion porosimetry (MIP) is carried out by using the Micromeritrics Autopore porosimeter. For these tests, one fragment (dimension ≈ 1 cm^3) is selected by each sample for which sorptivity has been estimated by capillary absorption test.

4. IFU Application and Comparison with Experimental and Model Findings

The comparison between experimental findings and modelling predictions can be used to validate the IFU modelling approach and tests its capabilities and limitations. In particular, Tables 1–4 show IFU input data to set the model in order to reproduce experimental porosimetric cumulative curves. They report the fractal dimension (D_f), the maximum (R_{max}) and minimum rays (R_{min}), the number (i) of iterations (R_{max}, R_{min}, and i strictly depends on experimental porometric data), the number of *solid forever* squares for each base unit (the Sierpinki carpet), the number of B base units (n_B), the filled surface (FS) used to build the IFU, and a comparison between experimental (ε_{exp}) and predicted (ε_{IFU}) porosities expressed as a fraction.

Figure 3 reports a comparison between experimental (from MIP tests [50, 51]) and modelling pore cumulative curves. The following graphs are given as an example for B-2, B-3; C-2, C-4; and D-3, D-4 systems.

It is possible to see that IFU modelling reproductions are in good agreement with experimental findings.

Once the simulation has been successfully performed, the IFU input data (from Tables 1–4) can be used to apply (14) for calculating the sorptivity values (S_{IFU}). The S_{IFU} has been compared in Table 5 with the corresponding experimental measurements (S_{exp}) [48–52].

Moreover, in order to make a comparison complete, Table 5 also contains the sorptivity calculated by adopting the models reported in [9], $S_{[9]}$, and in [12], $S_{[12]}$,

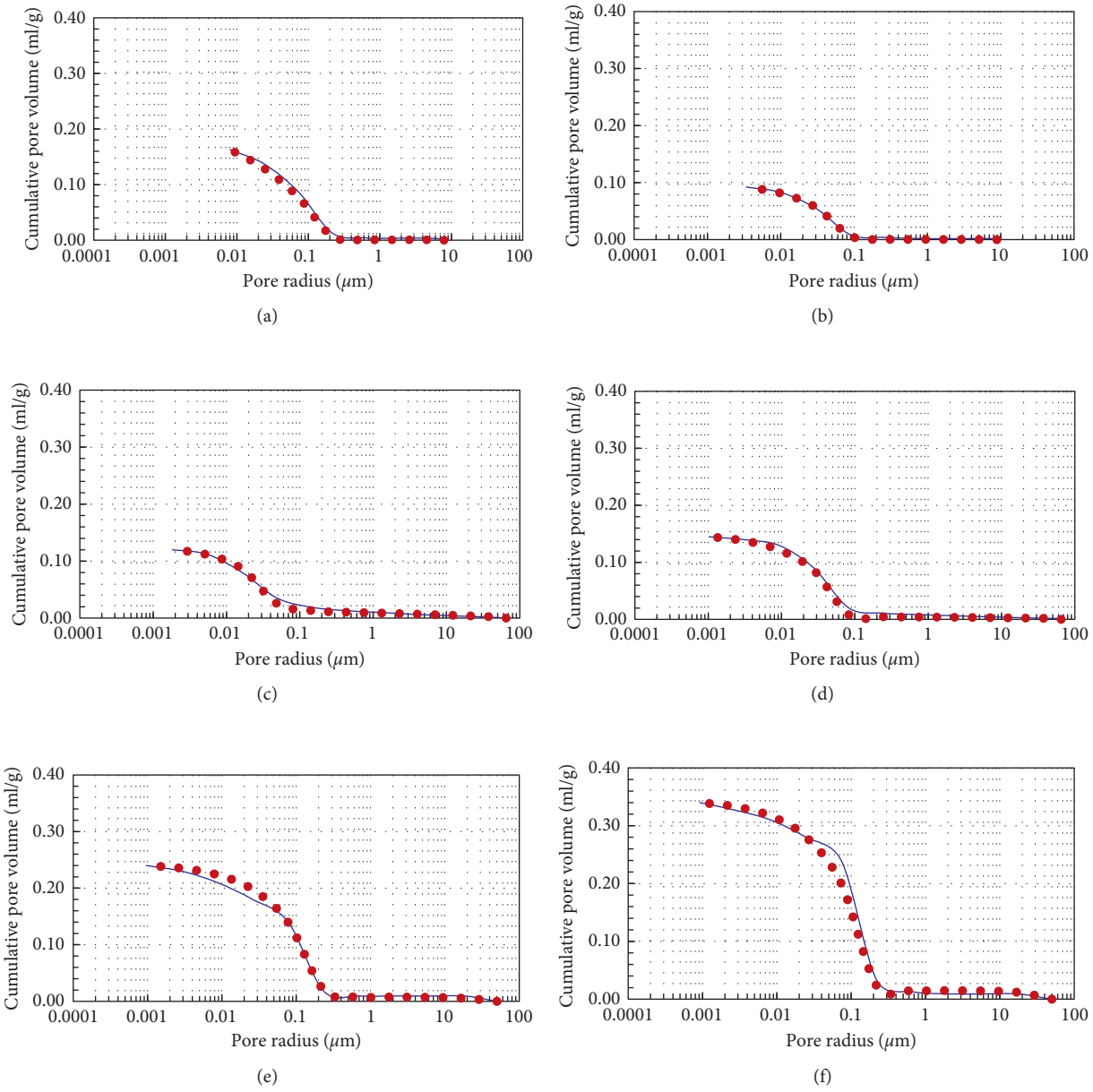

Figure 3: Comparison between experimental (continuous line) and IFU (dot line) pore cumulative curves: B-2 (a), B-3 (b), C-2 (c), C-4 (d), D-3 (e), and D-4 (f).

$$S_{[9]} = \rho\left(\frac{\gamma}{\mu}\right)^{0.5}\frac{\varepsilon_{\exp}}{\tau}r_0^{0.5}\left(\cos\frac{\theta}{2}\right)^{0.5},$$
$$S_{[12]} = \varepsilon\rho\sqrt{\frac{\varepsilon_{\exp}r\gamma\cos\theta}{5\mu}}, \quad (15)$$

where ρ, γ, μ, ε, r_0, τ, and θ represent, respectively, the density, the surface tension, the viscosity of the liquid, the experimental open porosity, the median pore size, the pore tortuosity of the solid, and the liquid-brick contact angle [9]. These models predict sorptivity values with two different analytical procedures. It is possible to note that $S_{[9]}$ and $S_{[12]}$ predictions are definitely much smaller or higher than the experimental findings. The greater difference obtained by applying the latter two procedures [9, 12] is presumably owing to the fact that they only take into consideration the mean pore radius, while the IFU procedure considers the whole pore size distribution. Indeed, pore size distributions can be very different from each other, and they can determine diverse properties and performances of porous materials [5, 29, 42, 43]. Nevertheless, these pore size distributions can have the same average pore radius.

Under these circumstances, since, for some materials, average pore radius can be representative of pore size distribution [9, 12], for others, it is necessary to consider entirely their pore size distribution.

Overall, the IFU modelling procedure proposed has proven to be an important tool to better understand the correlation between microstructures and suction properties

Table 5: Comparison among the sorptivity values obtained experimentally (S_{exp}), calculated on the basis of the IFU model (S_{IFU}) and the formulas proposed by Raimondo ($S_{[9]}$) and Scherer ($S_{[12]}$).

Sample	S_{exp} (mg cm^{-2} s$^{-0.5}$)	S_{IFU} (mg cm^{-2} s$^{-0.5}$)	$S_{[9]}$ (mg cm^{-2} s$^{-0.5}$)	$S_{[12]}$ (mg cm^{-2} s$^{-0.5}$)
A-1	5.59	4.34	10.42	37.78
A-2	8.83	6.19	10.75	345.94
B-1	0.42	0.97	5.03	2.68
B-2	0.80	1.51	10.97	5.31
B-3	0.92	1.60	24.46	23.11
C-1	5.71	6.44	39.90	2.47
C-2	2.29	4.93	42.80	5.25
C-3	3.28	4.84	31.35	5.68
C-4	3.81	2.92	63.12	5.12
D-1	2.20	3.84	5.32	6.72
D-2	7.20	9.35	11.94	9.44
D-3	16.90	19.94	10.28	23.39
D-4	35.00	32.20	21.20	33.51
D-5	51.00	50.68	79.40	114.69
D-6	59.00	59.53	91.77	66.45

of porous materials. It allows verifying the data achieved from experimental tests that are often difficult to implement and/or interpret. The IFU model has full potentiality to become a work instrument to plan the mix design of cement pastes.

5. Conclusions

An intermingled fractal units' model has been developed in order to reproduce the pore size distribution of cement. By applying an analytical-fractal procedure, it is possible to predict the sorptivity coefficient. The agreement between experimental findings and modelling predictions indicates that the IFU model developed is able to suitably account for the fundamental mechanisms of water absorption in porous building materials. Moreover, other two analytical procedures to have sorptivity values have been applied, but it is possibly established that the newly proposed method better matches with the experimental results. This good agreement achieved is probably due to the IFU capability to consider pore size distribution entirely and not only an average pore. In fact, the IFU model based on fractal units is able to reproduce every pore size distribution even if they are not fractal.

Conflicts of Interest

The authors declare that they have no conflicts of interest.

References

[1] C. Moses, D. Robinson, and J. Barlow, "Methods for measuring rock surface weathering and erosion: a critical review," *Earth-Science Reviews*, vol. 135, pp. 141–161, 2014.

[2] C. Cardell, F. Delalieux, K. Roumpopoulos, A. Moropoulou, F. Auger, and R. Van Grieken, "Salt-induced decay in calcareous stone monuments and buildings in a marine environment in SW France," *Construction and Building Materials*, vol. 17, no. 3, pp. 165–179, 2003.

[3] F. Sandrolini, E. Franzoni, E. Sassoni, and P. P. Diotallevi, "The contribution of urban-scale environmental monitoring to materials diagnostics: a study on the Cathedral of Modena (Italy)," *Journal of Cultural Heritage*, vol. 12, no. 4, pp. 441–450, 2011.

[4] O. Rudic, D. Rajnovic, D. Cjepa, S. Vucetic, and J. Ranogajec, "Investigation of the durability of porous mineral substrates with newly designed TiO_2-LDH coating," *Ceramics International*, vol. 41, no. 8, pp. 9779–9792, 2015.

[5] G. Pia and U. Sanna, "An intermingled fractal units model and method to predict permeability in porous rock," *International Journal of Engineering Science*, vol. 75, pp. 31–39, 2014.

[6] C. Atzeni, G. Pia, and U. Sanna, "A geometrical fractal model for the porosity and permeability of hydraulic cement pastes," *Construction and Building Materials*, vol. 24, no. 10, pp. 1843–1847, 2010.

[7] E. Franzoni, "Rising damp removal from historical masonries: a still open challenge," *Construction and Building Materials*, vol. 54, pp. 123–136, 2014.

[8] J. Cai, X. Hu, D. C. Standnes, and L. You, "An analytical model for spontaneous imbibition in fractal porous media including gravity," *Colloids and Surfaces A: Physicochemical and Engineering Aspects*, vol. 414, pp. 228–233, 2012.

[9] M. Raimondo, M. Dondi, D. Gardini, G. Guarini, and F. Mazzanti, "Predicting the initial rate of water absorption in clay bricks," *Construction and Building Materials*, vol. 23, no. 7, pp. 2623–2630, 2009.

[10] D. Park, S. Park, Y. Seo, and T. Noguchi, "Water absorption and constraint stress analysis of polymer-modified cement mortar used as a patch repair material," *Construction and Building Materials*, vol. 28, no. 1, pp. 819–830, 2011.

[11] M. Rabehi, B. Mezghiche, and S. Guettala, "Correlation between initial absorption of the cover concrete, the compressive strength and carbonation depth," *Construction and Building Materials*, vol. 45, pp. 123–129, 2013.

[12] G. W. Scherer and G. S. Wheeler, "Silicate consolidants for stone," *Key Engineering Materials*, vol. 391, pp. 1–25, 2009.

[13] Z. Wu, H. S. Wong, and N. R. Buenfeld, "Influence of drying-induced microcracking and related size effects on mass transport properties of concrete," *Cement and Concrete Research*, vol. 68, pp. 35–48, 2015.

[14] E. Franzoni, E. Sassoni, G. W. Scherer, and S. Naidu, "Artificial weathering of stone by heating," *Journal of Cultural Heritage*, vol. 14, no. 3, pp. e85–e93, 2013.

[15] M. Á. García-del-Cura, D. Benavente, J. Martínez-Martínez, and N. Cueto, "Sedimentary structures and physical properties of travertine and carbonate tufa building stone," *Construction and Building Materials*, vol. 28, no. 1, pp. 456–467, 2012.

[16] P. J. McGlinn, F. C. de Beer, L. P. Aldridge et al., "Appraisal of a cementitious material for waste disposal: neutron imaging studies of pore structure and sorptivity," *Cement and Concrete Research*, vol. 40, no. 8, pp. 1320–1326, 2010.

[17] M. Y. J. Liu, U. J. Alengaram, M. Z. Jumaat, and K. H. Mo, "Evaluation of thermal conductivity, mechanical and transport properties of lightweight aggregate foamed geopolymer concrete," *Energy and Buildings*, vol. 72, pp. 238–245, 2014.

[18] U. A. Dogan and M. H. Ozkul, "The effect of cement type on long-term transport properties of self-compacting concretes," *Construction and Building Materials*, vol. 96, pp. 641–647, 2015.

[19] Z. Zhang, "Comparisons of various absorbent effects on carbon dioxide capture in membrane gas absorption (MGA)

process," *Journal of Natural Gas Science and Engineering*, vol. 31, pp. 589–595, 2016.

[20] M. Rezakazemi, I. Heydari, and Z. Zhang, "Hybrid systems: combining membrane and absorption technologies leads to more efficient acid gases (CO_2 and H_2S) removal from natural gas," *Journal of CO_2 Utilization*, vol. 18, pp. 362–369, 2017.

[21] Z. Zhang, Y. Yan, L. Zhang et al., "Theoretical study on CO_2 absorption from biogas by membrane contactors: effect of operating parameters," *Industrial and Engineering Chemistry Research*, vol. 53, no. 36, pp. 14075–14083, 2014.

[22] A. Stazi, M. D'Orazio, and E. Quagliarini, "In-life prediction of hygrometric behaviour of buildings materials: an application of fractal geometry to the determination of adsorption and suction properties," *Building and Environment*, vol. 37, no. 7, pp. 733–739, 2002.

[23] B. B. Mandelbrot, *The Fractal Geometry of Nature*, Freeman, New York, NY, USA, 2004.

[24] S. Sasanian and T. A. Newson, "Use of mercury intrusion porosimetry for microstructural investigation of reconstituted clays at high water contents," *Engineering Geology*, vol. 158, pp. 15–22, 2013.

[25] L. Korat, V. Ducman, A. Legat, and B. Mirtič, "Characterisation of the pore-forming process in lightweight aggregate based on silica sludge by means of X-ray micro-tomography (micro-CT) and mercury intrusion porosimetry (MIP)," *Ceramics International*, vol. 39, no. 6, pp. 6997–7005, 2013.

[26] J. Zhou, G. Ye, and K. van Breugel, "Characterization of pore structure in cement-based materials using pressurization–depressurization cycling mercury intrusion porosimetry (PDC-MIP)," *Cement and Concrete Research*, vol. 40, no. 7, pp. 1120–1128, 2010.

[27] R. M. Novais, M. P. Seabra, and J. A. Labrincha, "Ceramic tiles with controlled porosity and low thermal conductivity by using pore-forming agents," *Ceramics International*, vol. 40, no. 8, pp. 11637–11648, 2014.

[28] C. Atzeni, G. Pia, and U. Sanna, "Fractal modelling of medium–high porosity SiC ceramics," *Journal of the European Ceramic Society*, vol. 28, no. 14, pp. 2809–2814, 2008.

[29] G. Pia, L. Casnedi, M. Ionta, and U. Sanna, "On the elastic deformation properties of porous ceramic materials obtained by pore-forming agent method," *Ceramics International*, vol. 41, no. 9, pp. 11097–11105, 2015.

[30] D. N. Winslow, "The fractal nature of the surface of cement paste," *Cement and Concrete Research*, vol. 15, no. 5, pp. 817–824, 1985.

[31] R. A. Livingston, "Fractal nucleation and growth model for the hydration of tricalcium silicate," *Cement and Concrete Research*, vol. 30, no. 12, pp. 1853–1860, 2000.

[32] D. A. Lange, H. M. Jennings, and S. P. Shah, "Image analysis techniques for characterization of pore structure of cement-based materials," *Cement and Concrete Research*, vol. 24, no. 5, pp. 841–853, 1994.

[33] S. Diamond and D. Bonen, "Microstructure of hardened cement paste. A new interpretation," *Journal of the American Ceramic Society*, vol. 76, no. 12, pp. 2993–2999, 1993.

[34] M. Arandigoyen and J. I. Alvarez, "Pore structure and mechanical properties of cement–lime mortars," *Cement and Concrete Research*, vol. 37, no. 5, pp. 767–775, 2007.

[35] V. Comegna, P. Damiani, and A. Sommella, "Use of a fractal model for determining soil water retention curves," *Geoderma*, vol. 85, no. 4, pp. 307–323, 1998.

[36] Y. F. Xu and P. Dong, "Fractal approach to hydraulic properties in unsaturated porous media," *Chaos, Solitons and Fractals*, vol. 19, no. 2, pp. 327–337, 2004.

[37] Y. Shi, J. Xiao, M. Pan, and R. Yuan, "A fractal permeability model for the gas diffusion layer of PEM fuel cells," *Journal of Power Sources*, vol. 160, no. 1, pp. 277–283, 2006.

[38] Q. Zheng and B. Yu, "A fractal permeability model for gas flow through dual-porosity media," *Journal of Applied Physics*, vol. 111, no. 2, p. 024316, 2012.

[39] C. Atzeni, G. Pia, U. Sanna, and N. Spanu, "Surface wear resistance of chemically or thermally stabilized earth-based materials," *Materials and Structures*, vol. 41, no. 4, pp. 751–758, 2007.

[40] X. Huai, W. Wang, and Z. Li, "Analysis of the effective thermal conductivity of fractal porous media," *Applied Thermal Engineering*, vol. 27, no. 17-18, pp. 2815–2821, 2007.

[41] J. Cai and X. Huai, "Study on fluid–solid coupling heat transfer in fractal porous medium by lattice Boltzmann method," *Applied Thermal Engineering*, vol. 30, no. 6-7, pp. 715–723, 2010.

[42] G. Pia and U. Sanna, "Intermingled fractal units model and electrical equivalence fractal approach for prediction of thermal conductivity of porous materials," *Applied Thermal Engineering*, vol. 61, no. 2, pp. 186–192, 2013.

[43] G. Pia, L. Casnedi, and U. Sanna, "Porous ceramic materials by pore-forming agent method: an intermingled fractal units analysis and procedure to predict thermal conductivity," *Ceramics International*, vol. 41, no. 5, pp. 6350–6357, 2015.

[44] G. Pia and U. Sanna, "A geometrical fractal model for the porosity and thermal conductivity of insulating concrete," *Construction and Building Materials*, vol. 44, pp. 551–556, 2013.

[45] G. Pia and U. Sanna, "An intermingled fractal units model to evaluate pore size distribution influence on thermal conductivity values in porous materials," *Applied Thermal Engineering*, vol. 65, no. 1-2, pp. 330–336, 2014.

[46] J. Comiti and M. Renaud, "A new model for determining mean structure parameters of fixed beds from pressure drop measurements: application to beds packed with parallelepipedal particles," *Chemical Engineering Science*, vol. 44, no. 7, pp. 1539–1545, 1989.

[47] P. Pfeifer and D. Avnir, "Chemistry in noninteger dimensions between two and three. I. Fractal theory of heterogeneous surfaces," *Journal of Chemical Physics*, vol. 79, no. 7, pp. 3558–3565, 1983.

[48] A. Bouguerra, H. Sallée, F. de Barquin, R. Dheilly, and M. Quéneudec, "Isothermal moisture properties of wood-cementitious composites," *Cement and Concrete Research*, vol. 29, no. 3, pp. 339–347, 1999.

[49] A. Bouguerra, A. Ledhem, F. de Barquin, R. M. Dheilly, and M. Quéneudec, "Effect of microstructure on the mechanical and thermal properties of lightweight concrete prepared from clay, cement, and wood aggregates," *Cement and Concrete Research*, vol. 28, no. 8, pp. 1179–1190, 1998.

[50] C. Atzeni, L. Massidda, and U. Sanna, "Densifying of cement pastes by chemical deposition of silica in the pores," in *Proceedings of International Congress on the Chemistry of Cement*, New Delhi, India, 1992.

[51] H. Garbalińska and A. Wygocka, "Microstructure modification of cement mortars: effect on capillarity and frost-resistance," *Construction and Building Materials*, vol. 51, pp. 258–266, 2014.

[52] M. Arandigoyen and J. I. Alvarez, "Blended pastes of cement and lime: pore structure and capillary porosity," *Applied Surface Science*, vol. 252, no. 23, pp. 8077–8085, 2006.